RESEARCH ARTICLE

A fast-integrated x-ray emission spectrometer dedicated to the investigation of Pt presence in gold Celtic coins (3rd–1st century BCE)

Anna Zymaková[1] | Vasiliki Kantarelou[1] | Stanislav Stanček[1,2] | Daniel Bursak[3] | Alžběta Danielisová[3] | Dimitrios F. Anagnostopoulos[4] | Martina Greplová Žáková[1] | Wojciech Błachucki[5] | Jakob Andreasson[1] | Daniele Margarone[1,6]

[1]ELI Beamlines Facility, The Extreme Light Infrastructure ERIC, Dolní Břežany, Czech Republic

[2]Joint Laboratory of Optics of Palacky University, Institute of Physics of Academy of Sciences of the Czech Republic, Faculty of Science, Olomouc, Czech Republic

[3]Institute of Archaeology of the Czech Academy of Sciences, Prague, Czech Republic

[4]Department of Materials Science and Engineering, University of Ioannina, Ioannina, Greece

[5]The Henryk Niewodniczański, Institute of Nuclear Physics, Polish Academy of Sciences, Krakow, Poland

[6]Centre for Light-Matter Interactions, School of Mathematics and Physics, Queen's University Belfast, Belfast, UK

Correspondence
Vasiliki Kantarelou, ELI Beamlines Facility, The Extreme Light Infrastructure ERIC, Za Radnicí 835, 252 41 Dolní Břežany, Czech Republic.
Email: vasiliki.kantarelou@eli-beams.eu

Abstract

With this study, we present the development of a transportable x-ray emission spectrometer (XES) that was realized in a net time of 20 h, in order to verify the presence of Platinum (Pt) in gold Celtic coins belonging to 3rd–1st century BCE. Prior to the XES study, measurements using Scanning Electron Microscopy coupled with Energy Dispersive Spectroscopy (SEM-EDS) revealed that the coins were made of highly concentrated gold (Au) alloy with trace amounts of bismuth (Bi) and, in one case, osmium (Os) and iridium (Ir). Os and Ir together with Pt and other components belong to the Platinum Group Elements (PGE). They form inclusions in ancient gold alloys and their presence is significant in provenance studies since they indicate the use of alluvial gold. Detection of platinum trace elements in a golden matrix is not possible using energy dispersive x-ray emission techniques (SEM-EDS, ED-XRF, or PIXE) because of the limited energy resolution of the Si detectors. A way to overcome this problem is by using a high-resolution wavelength dispersive x-ray emission technique. For this purpose, we built a crystal spectrometer in Von-Hamos geometry. In the framework of this study three samples/coins have been measured, and the presence of Pt was verified in one of them. The limitations of our spectrometer are critically evaluated and ways to optimize the performance of the spectrometer are discussed.

KEYWORDS
ancient gold inspection, detection of Pt in Au alloys, non-destructive analysis, platinum group mineral (PGM) inclusions, X-ray emission spectroscopy

1 | INTRODUCTION

Measurement of the composition of ancient gold coins has recently been carried out at the ELI-Beamlines facility (https://www.eli-beams.eu/) collaboratively with the Institute of Archaeology of the Czech Academy of Science (ARUP). Gold (Au) Celtic coins from the late Iron Age (3rd–1st century BCE) were used for elemental analysis. Scanning Electron Microscopy coupled with Energy Dispersive Spectroscopy (SEM-EDS) analyses showed that most of the coins were made of pure (or purified) gold alloys with a high Au content (Au > 95% wt., Ag < 5% wt., Cu < 1% wt.), trace amounts of bismuth (Bi) and in one case osmium (Os) and iridium (Ir).

Trace elements in gold, including Pt, Pd, Ag, Cu, Ni, Zn, Fe, Pb, and Sn, together with micro-inclusions of Platinum Group Mineral (PGM) composed of minerals grains insoluble in gold, indicate provenance of the gold from secondary deposits within stream sediments.[1–6] Quantification of trace elements in the gold is of key importance as their concentration does not change with melting, although oxidizing, reducing melting conditions or alloying might introduce alterations.[6] Detection and quantification of these trace elements can increase possibilities for provenance investigations by identifying the alluvial/placer or primary mining deposits of the gold, instead of geological fingerprints.[3,6–8]

The importance of the detection of Pt traces in gold objects was highlighted by Radtke et al.[9] The presence of Pt in gold leaves used for gilding the Abydos and Byzantine mosaics provided vital information indicating the alluvial origin of the gold and showed that the presence of Pt can be used as a criterion for provenance and dating ancient productions, even in the case of very thin gold layers. Radtke et al. concluded that workshops producing both the gold Egyptian leaves and the jewelry had the same suppliers. Moreover, the determination of Pt in such small and thin leaves opened new opportunities for dating ancient mosaics. The amount of Pt in the gold leaves of a statistically significant group of tesserae can be related to Byzantine gold coins, providing reliable future dating criteria. In another study[10] the major, minor and trace elements for a variety of gold samples from the Xiongnu necropolis in Mongolia were determined. The presence of Pt and Sn showed that, contrary to what was expected, the gold foils from the first powerful empire of the steppes along the Great Wall (2nd century BCE) were produced with alluvial gold from local placer deposits located in Mongolia Zaamar, Boroo and the Selenga River.

Micro-inclusions of PGM that include Os, Ir and Ru were found in gold artifacts from Asia Minor and Egypt[1,4,11] but also in the gold objects from Varna 1 cemetery in Bulgaria (4550–4450 BCE).[3] PGM are equally present in Celtic gold coins that were circulated in central Europe during the 2nd century BCE.[8] Concentrations, in ppm, of Pt vary depending on the area 21–99 in Sicily, 328–366 in Byzantine regions, 110–366 in Arab territories, 184–555 in Syria[12] reaching the highest amounts (<1200) at Ur in Mesopotamia[1] and 1095–1127 in Cambodia.[13]

Thus far no PGM micro-inclusions were reported in bibliography of golden samples, which contain <100 ppm Pt.[14] However, when Pt is present in concentrations higher than 100 ppm in gold, PGM inclusions might be present for example at Ur in Mesopotamia,[1] although exceptions have been noted.[12] Furthermore, Pt is usually present in higher amounts in gold alloy compared to other PGEs.[14] This was attributed to the different melting points among the PGEs and thus their different degree of solubility. Molten gold can assimilate 10% of Pt and 2.86% and 2.78% of Os and Ru, respectively. This supports the observation that inclusions consist mostly of Os, Ir and Ru rather than Pt. The Os-Ir-Ru inclusions in placers most commonly form grains of sizes between 30 and 50 μm and only rarely larger than 100–150 μm whereas Pt rich minerals form much larger grains which were extracted from placers along with gold.[14]

The large variability in the chemical composition of PGE inclusions does not allow a distinction between artifacts from different archeological deposits or periods.[4] However, the detection of other trace elements can improve provenance investigation by identifying different production cycles instead of geological fingerprints.[1,3,14–16]

The analytical techniques applied to detect trace impurities in gold have been reviewed by Guerra and Calligaro.[17] Among them, the most sensitive methods to detect Pt are Inductively Coupled Plasma-Mass Spectroscopy (ICP-MS) and Proton Activation Analysis (PAA). PAA is based on the bombardment of an object with a proton beam and measurement of the delayed gamma radiation emitted by the radionuclide. It offers detection limits in the range of a few parts per million. ICP-MS is more sensitive and is normally used to determine a very wide range of trace elements in gold at very low concentration levels. Limits of detection vary from 0.01 to 10 ppb. The main drawback of PAA is induced radioactivity, which makes it unsuitable for exhibited artifacts. On the other hand, ICP-MS is a micro-destructive technique as it needs either to dilute a minimum amount of mass or (in the case of Laser Abletion ICP-MS) consume it by the laser beam. PIXE and XRF are non-invasive approaches that, even with the use of Zn filter to reduce the Au peak residual background, do not exhibit the

required sensitivity to detect Pt below 0.1% wt.[18,19] Spatially resolved synchrotron based XRF (Sy-XRF) analysis has been proven to be an ultimate choice for Pt analysis attaining a minimum detection limit of 0.9 ppm by means of Double Dispersive x-ray Fluorescence (D2XRF) analysis based on an Energy Dispersive pnCCD detector.[9]

However, the application of this technique, commonly used for synchrotrons, requires the transfer of objects to specialized large-scale facilities. In our case, the transport of precious and unique coins from the National Museum of Prague was not feasible, for security reasons. Therefore, a modular fast integrated x-ray spectrometer was built at the nearest available site offering suitable x-ray shielding conditions ELI Beamlines located in close vicinity of Prague.

Wavelength Dispersive X-ray Fluorescence (WDXRF) analysis was applied for Pt trace element analysis in gold objects. Pt was detected in ancient Roman gold coins with a concentration of ~300 ppm.[20] The detection limits of the method were estimated to 20 ppm, while quantification can be accurate at 70 ppm level. Some of the aforementioned coins were also selected for rapid quantitative mapping of Pt[21] using synchrotron radiation induced XRF analysis combined with a Wavelength Dispersive spectrometer.

Recently XES stations have appeared in laboratories as stationary or portable systems.[22,23] In XES primary hard x-rays originating from an x-ray source irradiate a sample and the emitted x-rays are collected by a single or multiple bent crystals,[24–27] that are arranged in Johann, Johansson, or Von Hamos configurations. In the Von Hamos geometry,[28] a cylindrically-bent crystal disperses the radiation along its flat surface's plane and focuses it along its axis of curvature forming a 1D matrix of photons resolved by energy/wavelength. The wavelength-dispersed spectrum was recorded using a one- or two-dimensional pixel x-ray detector. Current-generation solid-state detectors and the development of low-power micro-focus x-ray tubes, cylindrically or even spherically-bent[29] crystal analyzers (SBCA) now allow the XES method to be feasible away from synchrotron facilities.[30]

With this work, we present a study of ancient Celtic coins performed using a transportable fast-integrating high resolution x-ray emission spectrometer (XES).

2 | MATERIALS AND METHODS

2.1 | The golden coins

In this study, 25 Au Celtic coins from the Iron Age (3rd–1st century BCE) from the collections of the National Museum of Prague were measured. They were cast in clay molds, are of slightly concave shape resulting from the impact of the punch with a diameter of 0.5–1 cm.

Samples were first examined by Scanning Electron Microscopy (SEM-EDS) at the Faculty of Science, Charles University in Prague. Figure 1a shows a microscopic picture of sample Au28, with the depiction of a stylized Sun. No specific pattern is expected on Celtic coin decorations since they followed the predominant trend in the particular ancient trading area to which the territory of the issuing tribe belonged.[31] In the red square, the position of an inclusion is reported, whereas in Figure 1b a zoom in on the micro-inclusion is displayed.

SEM-EDS analyses were performed on different areas of all coins providing the overall composition of the alloy used. The coins were made of a high concentration gold alloy (i.e., pure or purified gold): Au > 95% wt., Ag < 5% wt. and Cu < 0.8% wt. with trace elements of Fe, Ni, Bi and in one case (Au28 in Figure 1), Ir and Os were detected in the area of the inclusion. Low concentrations of Cu and Ag indicate the use of a "pure" alloy and not one artificially made or recycled one.

FIGURE 1 SEM pictures of the sample Au28, (a) the entire surface of the coin is documented, an inclusion is present in the highlighted red area (b) the inclusion has an irregular shape and the max width and height is approximately 20 and 50 μm, respectively.
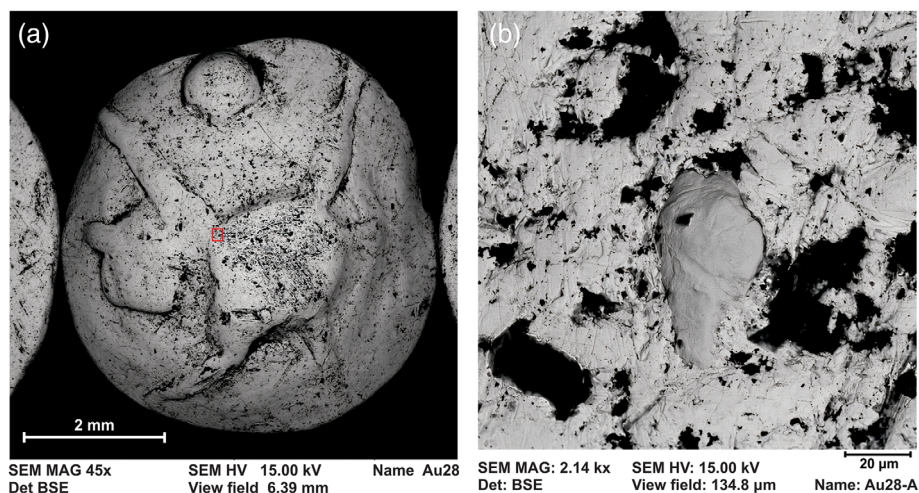
A restriction in archaeometric studies is the limited time for examination outside the storage/exhibition place of the artifacts and prohibition of destructive examinations. In our case, 1 week was given to examine the gold coins in our laboratory at ELI-beamlines. Because of the need to develop and optimize the method, we decided to analyze three of them where micro-inclusions were observed during SEM analysis.

2.2 | The X ray emission spectrometer

The main problem in the detection of Pt in a gold alloy with ED-XRF and PIXE techniques is the limited energy resolution of Si-based detectors, especially when Pt is present in low concentrations (below 1% wt.). A way to experimentally demonstrate the contribution of Pt-Lα lines in the ED-XRF spectrum from a binary Au-Pt alloy is by measuring pure Au and Pt targets and adding their respective spectra. The measurement times could be adjusted to imitate the concentration inside the hypothetical binary alloy. For this reason, pure Au and Pt targets were measured with a M1 Mistral, Bruker, ED-XRF

spectrometer equipped with a W anode tube (50 kV, 800 μA) and a SDD (30 mm^2). Figure 2a–c show the individual spectra from pure Au, pure Pt, and their addition. With equal amounts of Pt and Au, the detection of the Pt-Lα line is straightforward (Figure 2a). In the case of a binary Pt-Au alloy with 1% wt. Pt, the Pt-Lα line appears as a shoulder to the low energy side of the Au-Lα line, (Figure 2b). However, when the Pt content is 0.1% wt., the Pt-Lα line is completely hidden inside the Au-Lα line (Figure 2c). This limitation in conventional ED-XRF analysis can be successfully overcome through the application of high-energy resolution XES.

A von Hamos x-ray spectrometer is a chemical speciation sensitive setup based on Bragg's law and has energy resolution of <<1 eV. This allows for the resolution of closely appearing characteristic emission lines of chemical elements such as Pt and Au Lα lines. The XES spectrometer for this experiment had total dimensions of not more than 1 m × 1 m × 70 cm (excluding the shielding of the station) and was assembled in 20 h. The setup was composed of components already available at the facility, because it was a temporary and rapidly implemented solution. The spectrometer comprised three main compact units:
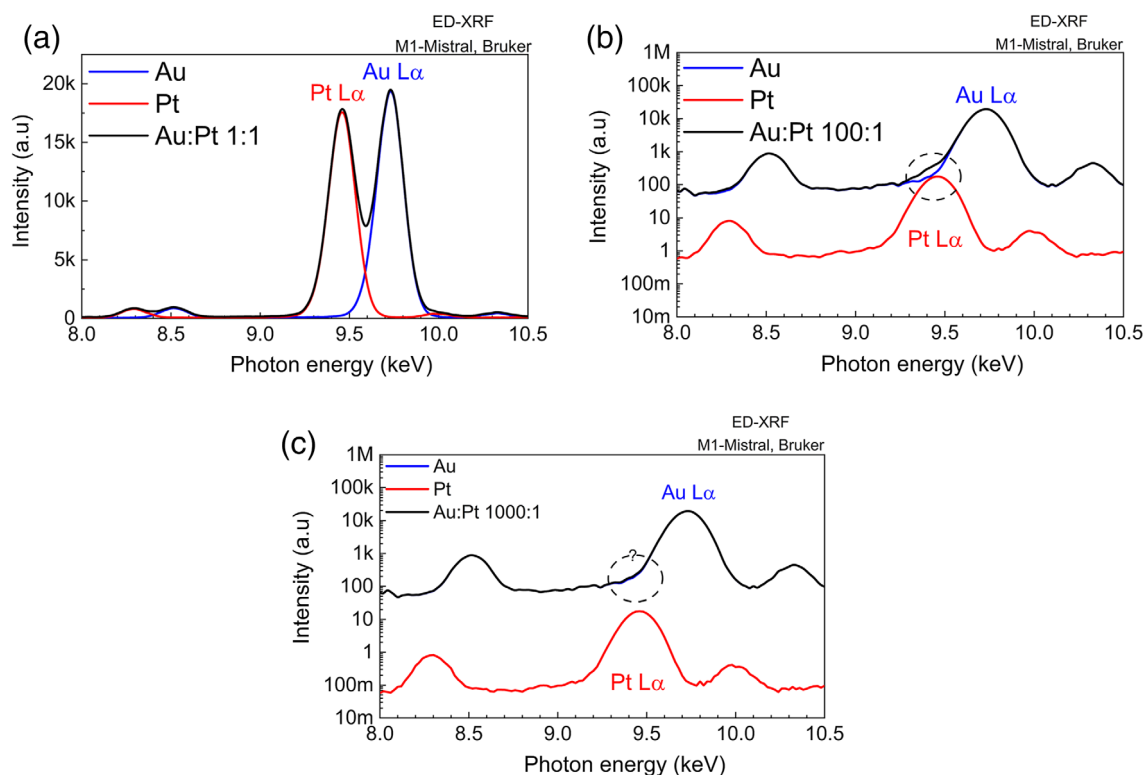

FIGURE 2 (a–c) ED-XRF spectra from pure Au and Pt targets, recorded by the M1-Mistral instrument, Bruker. The measurement time of each spectrum was altered so that the relative concentration of a hypothetical binary (Au-Pt) alloy was imitated. (a) In the case of an equal amount of Au and Pt the detection of Pt is straightforward. (b) If the amount of Pt is 1/100 that of Au then only a tiny shoulder is recognizable at the "tail" of the Au-Lα line. (c) When the amount of Pt is 1/1000 that of Au, its signal is hidden below the Au-Lα line.

- a Rh anode water cooled x-ray source (100 W, 50 kV, 127 μm Be window) (Oxford Instruments, Neptune 5200 Series), the beam is focused by a Cu collimator with an opening of 500 μm which creates a spot beam with a diameter of 1 mm at the sample position (2 cm),
- a curved Si crystal (111),
- a position sensitive x-ray detector - front illuminated CCD camera, 2048 × 2048 active pixels, $13.5 \times 13.5~\mu m^2$ pixel size (Andor's iKon-M).

The configuration of the XES is depicted in Figure 3. Positions of the analyzer and the detector were calculated to fulfill the conditions for Bragg's diffraction of the energy of interest (Pt-Lα_1) and the focusing radius of the crystal ($R = 250$ mm). The analyzer crystal and the CCD camera were mounted on stepper motors that allow for remote fine alignment of these components whereas the x-ray tube was in a fixed position. The sample was positioned on the same plane as the CCD and parallel to the crystal. The x-ray tube was at 45° with respect to the surface of the sample. This setup provided an energy band of 223 eV.

The absolute position of the crystal was fine-tuned by changing the position of the motors during the measurement of the thin Pt foil. In the final geometry, the Pt-Lα_1 signal recorded by the CCD camera was maximized. In Figure 4 the distributions of the photon counts after the integration of 220 frames at three positions of the crystal (spots 1, 2, 3) are presented whereas Figure 4d shows the corresponding spectra. The
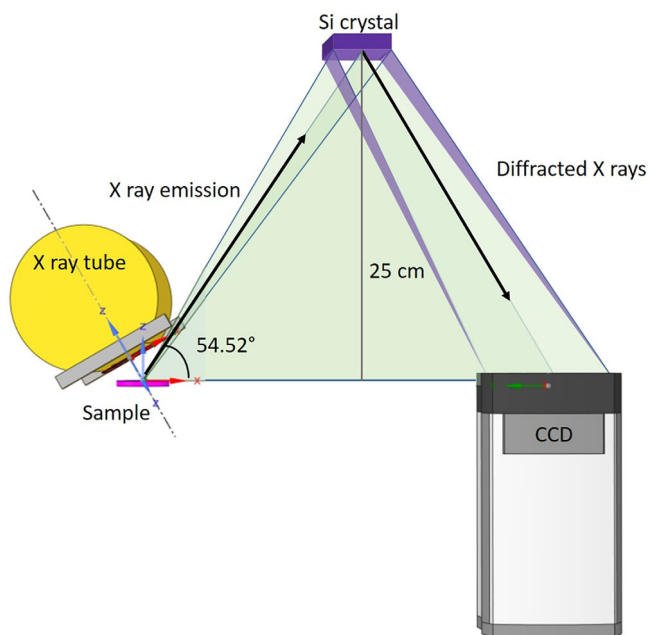
maximum counts in the Pt-Lα_1 line are detected in spot 2 where the second line Pt-Lα_2 is also starting to appear. This second line is the verification of the Pt signal, which was further improved by micro-changes in the position of the CCD camera. The peak to background ratio was enhanced by inserting Al foils along the path of the x-rays and in front of the CCD camera to avoid unwanted radiation. Figure 5 presents the final geometry of our spectrometer where the path of the x-rays is illustrated by green arrows. At the final position, the Pt foil was measured once more for 2 h resulting in a more intense signal on the CCD (Figure 6a). In the spectrum that was built after integration of 2000 frames the presence of Pt-Lα_2 is now evident.

3 | RESULTS

Three samples were analyzed from the collection of Celtic coins (Figure 7), Au17, Au20 and Au28. Different areas of the obverse and reverse of the coins were examined. A laser determined the area of analysis. The alignment of the laser was checked using radio-chromic film (RCF) that was placed in front of the sample. The x-rays emitted from the tube blackened the irradiated area on the surface of the RCF and afterwards the laser was aligned on the black spot.

From these samples, Pt was detected in Au28 in the area of the inclusion. Figure 8a presents the image from the CCD camera with integrated data from 2100 frames (corresponding to a measurement of 2 h). Overlapped spectra from Au28 and the Pt-foil (Figure 8b) show that the Pt-Lα_1 peak is slightly shifted (by 2 eV) for Au28. This can be attributed to geometrical reasons since the surface of the inclusion is not flat.

The inset of Figure 8b shows a zoom in of the region with the Pt-Lα_1 emission where an elevated background is observed in the case of Au28. This background signal is related to Au-Lα_1 emission from the sample since the size of the beam covers a more extensive area than the PGM "island" with an irregular shaped surface with max width of 20 μm and height of 50 μm.

To produce quantitative results three gold alloy reference samples with traces of Pt that varied from 600 to 1500 ppm were purchased from SAFINA, a.s. The reference sample with the higher concentration of Pt (64.2% wt. Au, 24.7% wt. Cu, 9.7% wt. Ag, 0.15% wt. Pt) was measured on the surface by single spot measurements and on a cross section by a line scan that covered the whole area during an over-night (10 h) measurement (Figure 9). Pt was not detected in either case, probably since Pt in the reference sample is evenly distributed inside the gold alloy (not forming inclusions/islands as in the case of
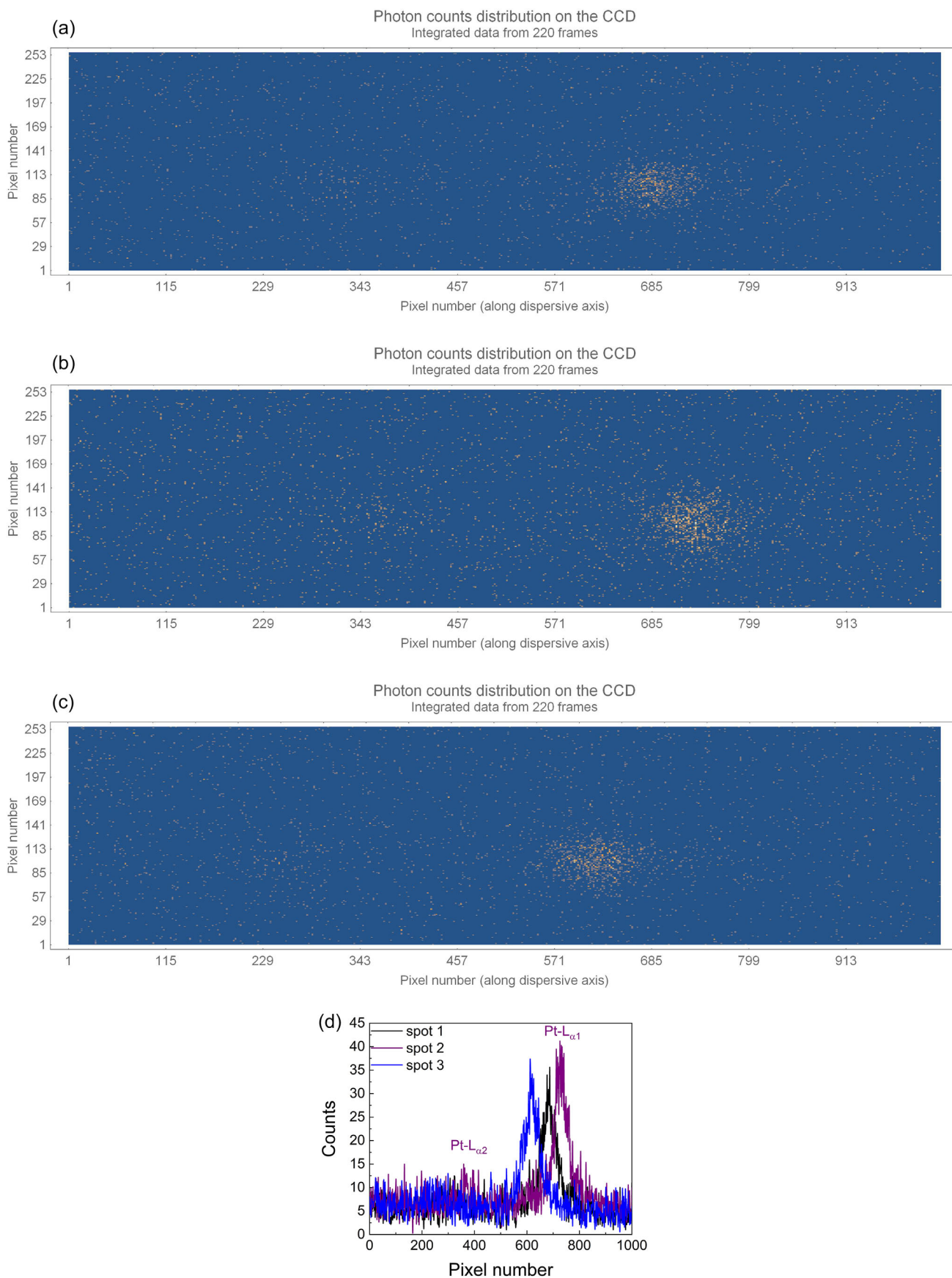

FIGURE 3 Schematic presentation of the Von-Hamos spectrometer.

ZYMAKOVÁ ET AL.

(a)

Photon counts distribution on the CCD
Integrated data from 220 frames

(b)

Photon counts distribution on the CCD
Integrated data from 220 frames

(c)

Photon counts distribution on the CCD
Integrated data from 220 frames

(d)

FIGURE 4   (a–c) Images from the CCD camera gained at three different spots by changing the position of the crystal, integrated data from 220 frames. (d) Spectra from the three different spots; spot 2 exhibits the maximum count rate in the Pt-Lα_1 line. In the same spot, the second line Pt-Lα_2 starts to appear.
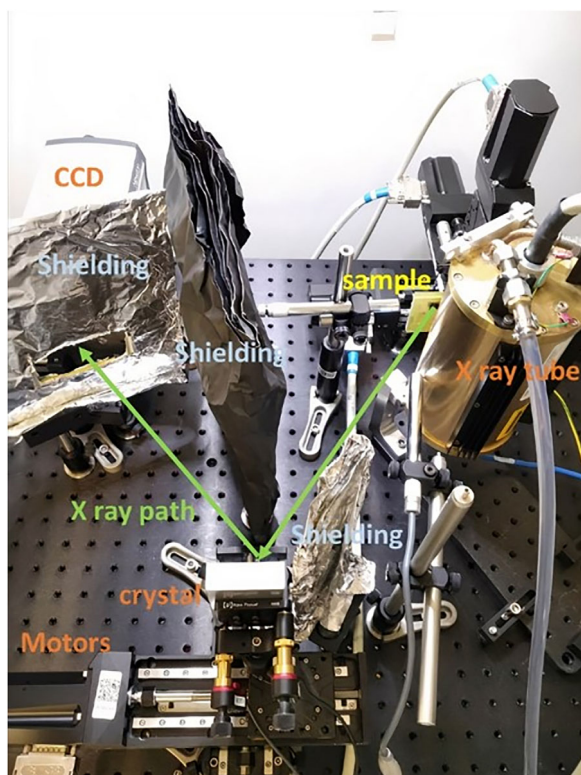
FIGURE 5 The x-ray emission spectrometer, in von-Hamos geometry. The path of the x-rays from the sample to the crystal analyzer and from the crystal to the detector are presented with green arrows.

Celtic coins) resulting in a higher contribution from the Au-Lα_1 signal.

To understand the lack of Pt signal, we applied a ray-tracing code for Von-Hamos spectrometers to simulate the spectrometer's response.[32] The geometry of the set-up, the target geometry, the crystal analyzer characteristics, the parameters of the CCD camera and the concentration of the sample (pure Au with 0.1% wt. Pt) were set as input parameters for the software. Figure 10 presents the simulated spectrum showing that the detection of a Pt-Lα_1 line at this concentration is possible, over the background produced by the "tail" of Au-Lα lines. At this point, we emphasize that the simulation does not have any source contributing to the background. This implies that we cannot consider all factors that might further elevate the background and eventually "hide" the Pt-Lα_1 peak. For example, the CCD camera that was used is a customized device that because of construction reasons can be cooled to $-50°$C and not below ($-80°$C or $-100°$C as is more usual for these detectors). This relatively high temperature is another reason for an increased background.

A weakness of the present setup is the relatively large source size and the resulting decrease in spectral resolution. The beam is focused by a Cu pinhole placed in front of the x-ray tube and the sample was placed 2 cm away resulting in an irradiation area with a diameter of
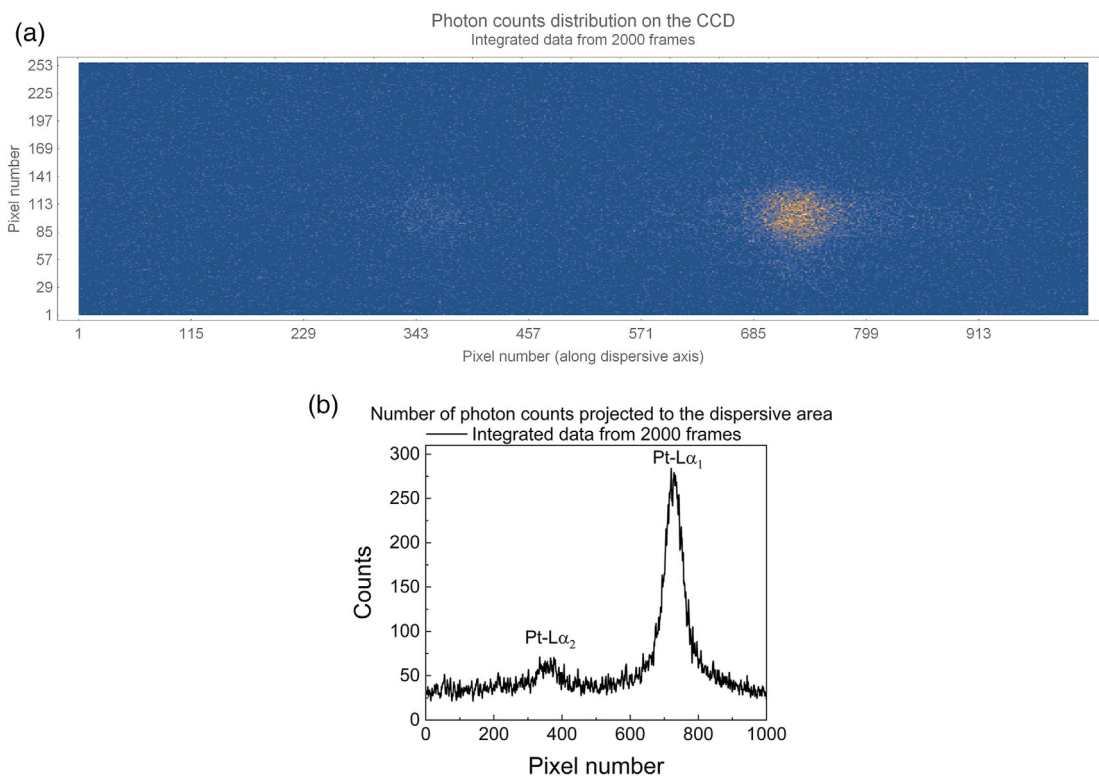

FIGURE 6 (a) Image from the CCD camera, the counts that correspond to the Pt-Lα_1 line are more intense and more focused than before (spots 1, 2, 3). (b) In the spectrum the presence of both Pt Lα_1 and Lα_2 lines is evident.
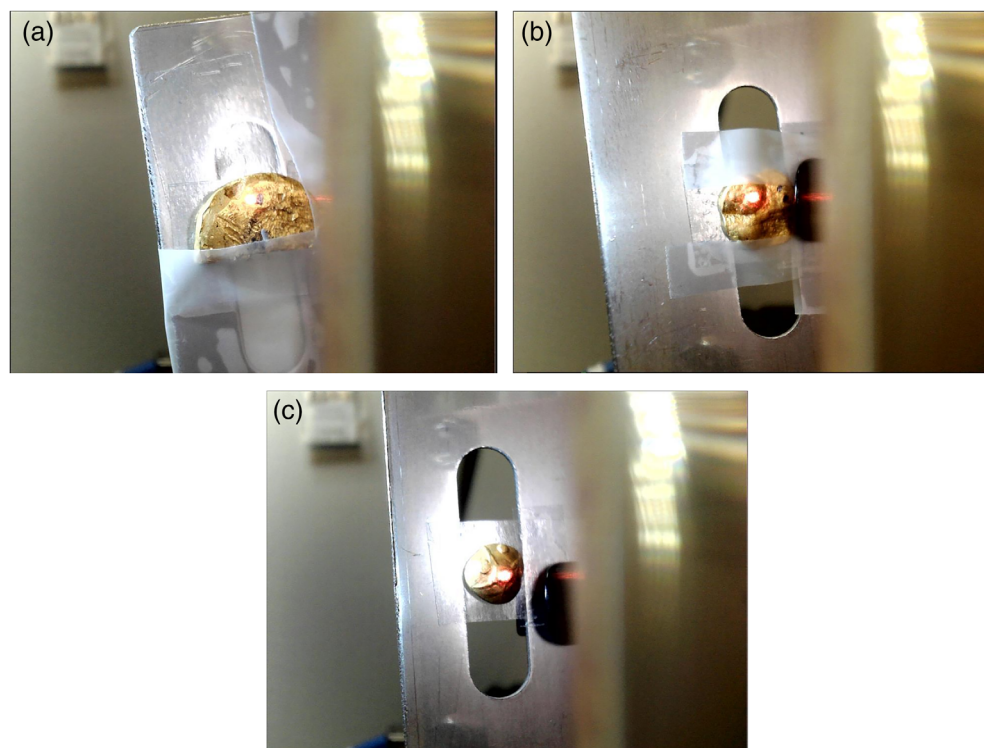
FIGURE 7 The gold coins (a) Au17, (b) Au20, (c) Au28, were placed on holders during the measurements. The laser spot on the sample that is visible in each picture was used to determine of the area of analysis.
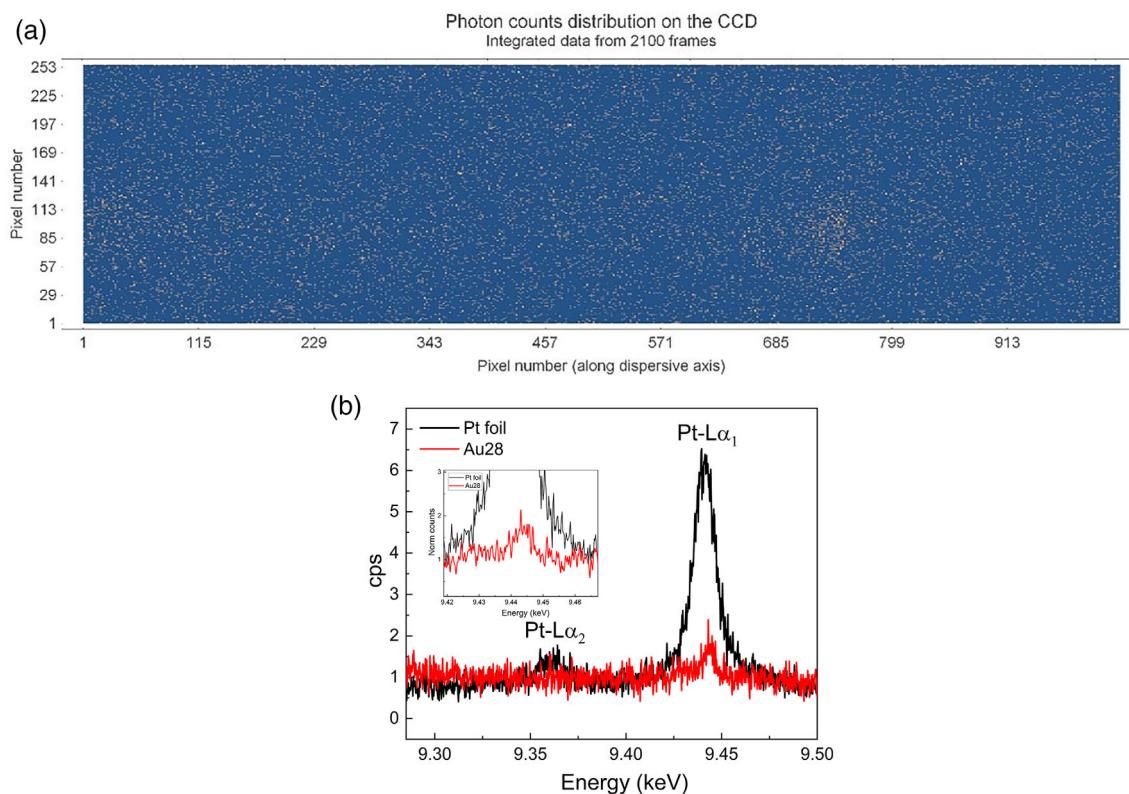

FIGURE 8 (a) Image of the CCD camera after integration of 2100 frames. (b) Spectra from a Pt foil and the inclusion of Au28, the y-axis presents the counts per second whereas in the inset, a magnification in the region of the Pt-Lα_1 is displayed.

approximately 1 mm. This has to be considered as a "large" source for XES, decreasing correspondingly the resolution of the spectrometer.

A simulation was made to validate the impact of the beam spot size on the resolution of the spectrometer. Figure 11 presents simulated spectra of a pure Pt target for a beam spot size of 5, 1 and 0.1 mm and it show that the energy resolution of the spectrometer can be significantly improved by decreasing the spot size. The full width at half maximum (FWHM) of the peak decreased by 60% when the beam size was reduced from 5 to 1 mm and by 13% from 1 to 0.1 mm. This improvement can be achieved by the use of a slit between the sample and the crystal analyzer or by using a micro-focusing x-ray tube or a focusing unit, for example a polycapillary x-ray lens[33] which can focus down to a few tens of micrometers, appropriate for high-resolution XES experiments.
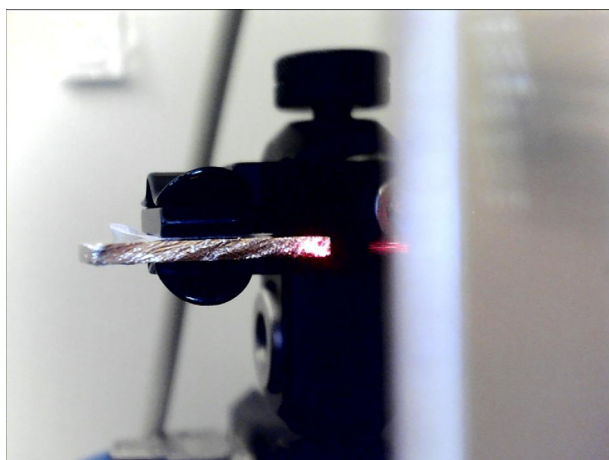

FIGURE 9 Reference sample examined by a line scan across a cross section.
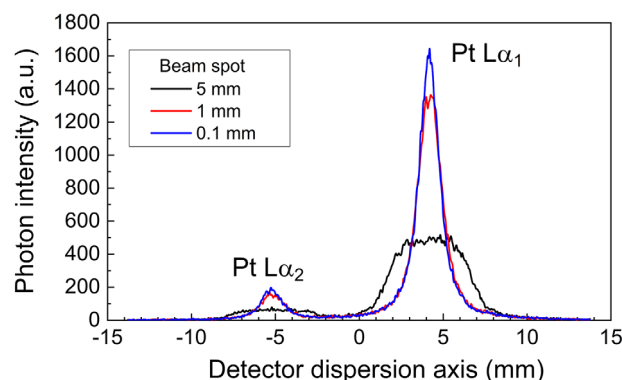

FIGURE 11 Pt L$\alpha_{1,2}$ simulated spectra as a function of the beam spot size for the Von-Hamos spectrometer's configuration. The impact of the beam spot on the spatial resolution, and consequently on the energy resolution, is noticeable.

FIGURE 10 Simulated XES spectrum from the Von-Hamos spectrometer of a gold sample with 0.1% wt Pt. The presence of Pt-Lα_1 is undoubtedly observed. Pt-Lα_2 transition is not distinguished in the low energy side of the Pt-Lα_1, as its intensity is about 10% of the Lα_1 intensity.
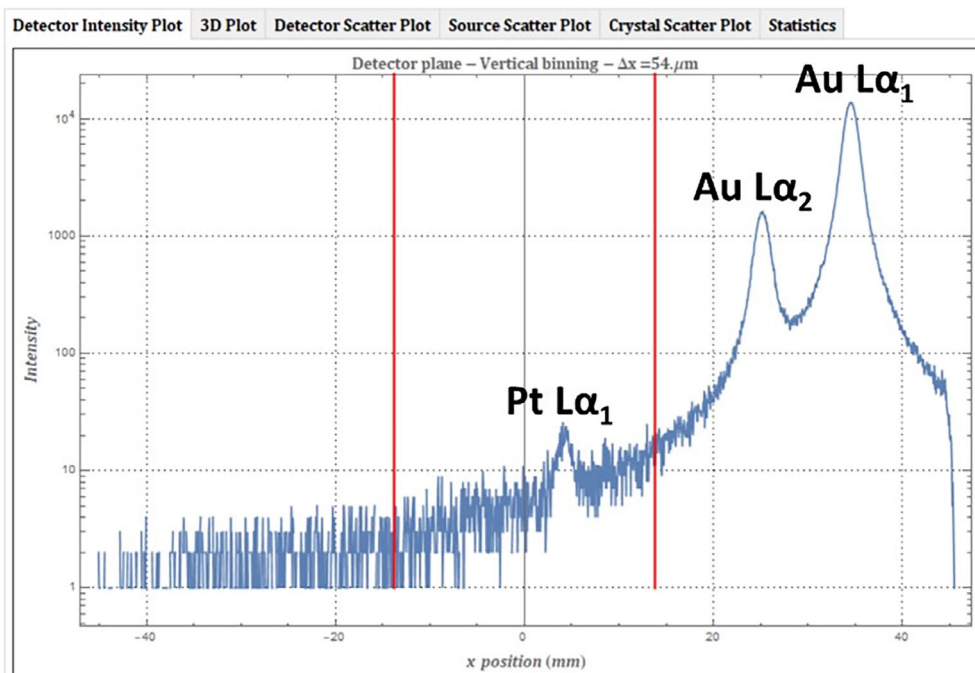
4 | CONCLUSIONS

Within this study, a portable and rapidly deployable XES was assembled to address the problem of the detection of Pt traces inside the alloy of gold Celtic coins. The presence of Pt was verified in one of the samples that contain a PGM inclusion. In the future, the study will be expanded to cover the entire collection of Celtic coins. In the described experiment, data quality was limited by the energy resolution of the rapidly constructed system. The analytical capabilities of the spectrometer were simulated, and its limitations were explored. In the next step, the energy resolution and data acquisition rate will be improved by the use of x-ray focusing optics with a ~100 μm focal spot diameter that will drastically enhance the photon flux over the exposed sample area.

This study is an important proof-of-principle for the possibility to conduct non-destructive analysis of precious artworks and culturally valuable artifacts at the site of the artifact, when long-distance transportation is undesirable, for example, due to security concerns. A chemically-sensitive compact von Hamos setup requires three key elements (an x-ray source, a small lightweight focusing crystal and a position-resolving detector) placed on a table surrounded by appropriate shielding walls. The experimental geometry is robust, and necessary shielding material can normally be found at institutes or hospitals near the site of the investigation. The construction takes less than half a day for a trained operator and can, in principle, be realized directly at the museum premises.

DATA AVAILABILITY STATEMENT

The data that support the findings of this study are available from the corresponding author upon reasonable request.

ORCID

Vasiliki Kantarelou https://orcid.org/0000-0003-0341-0016

Wojciech Błachucki https://orcid.org/0000-0003-4457-2345

REFERENCES

[1] M. Jansen, S. Aulbach, A. Hauptmann, H. E. Höfer, S. Klein, M. Krüger, R. L. Zettler, *J. Archaeol. Sci.* **2016**, *68*, 12.

[2] Q. Lemasson, B. Moignard, C. Pacheco, L. Pichon, M. F. Guerra, *Talanta* **2015**, *143*, 279.

[3] V. Leusch, B. Armbruster, E. Pernicka, V. Slavčev, *Cambridge Archaeol. J.* **2015**, *25*, 353.

[4] N. D. Meeks, M. S. Tite, *J. Archaeol. Sci.* **1980**, *7*, 267.

[5] E. Pernicka, *Mitteldeutscher Archäologentag* **2014**, *17*, 19.

[6] E. Pernicka, *Archaeometall. Glob. Perspect. Methods Syntheses* **2014**, *9781461490*, 259.

[7] S. C. Jensen, B. Sullivan, D. A. Hartzler, Y. Pushkar, *X-Ray Spectrom.* **2019**, *48*, 336.

[8] E. Pernicka. Tagungen des Landesmuseums für Vorgeschichte Halle Band 11/I | 2014 Metals of power – Early gold and silver, 6th Archaeological Conference of Central Germany, 2014, 153.

[9] M. Radtke, I. Reiche, U. Reinholz, H. Riesemeier, M. F. Guerra, *Microchem. J.* **2016**, *85*, 56.

[10] M. Radtke, I. Reiche, U. Reinholz, H. Reiesemeier, M. F. Guerra, *Anal. Chem.* **2013**, *125*, 1650.

[11] J. M. Ogden, *J. Egypt. Archaeol.* **1976**, *62*, 138.

[12] A. Gondonneau, M. F. Guerra, *Archaeometry* **2008**, *44*, 573.

[13] S. Schlosser, A. Reinecke, R. Schwab, E. Pernicka, S. Sonetra, V. Laychour, *J. Archaeol. Sci.* **2012**, *39*, 2877.

[14] V. V. Zaykov, I. Y. Melekestseva, E. V. Zaykova, D. Fellenger, D. Motz, *Archaeometry* **2018**, *60*, 1290.

[15] A. Hauptmann, in *Archaeometallurgy in Global Perspective* (Eds: B. W. Roberts, C. P. Thornton), Springer Science, New York **2014**, p. 91.

[16] V. V. Zaykov, V. A. Kotlyarov, E. V. Zaykova, I. Y. U. Melekestseva, *Archaeometry* **2017**, *59*, 96.

[17] M. F. Guerra, T. Calligaro, *J. Archaeol. Sci.* **2004**, *31*, 1199.

[18] M. F. Guerra, T. Calligaro, M. Radtke, I. Reiche, H. Riesemeier, *Nucl. Instrum. Methods Phys. Res. Sect. B Beam Interact. Mater. Atoms* **2005**, *240*, 505.

[19] M. F. Guerra, *Nucl. Instrum. Methods Phys. Res. Sect. B Beam Interact. Mater. Atoms* **2004**, *226*, 185.

[20] M. W. Hinds, G. Bevan, R. W. Burgess, *J. Anal. At. Spectrom.* **2014**, *29*, 1799.

[21] L. L. Van Loon, N. R. Banerjee, M. W. Hinds, R. Gordon, G. Bevan, R. W. Burgess, *J. Anal. At. Spectrom.* **2018**, *33*, 1763.

[22] J. Szlachetko, M. Nachtegaal, E. de Boni, M. Willimann, O. Safonova, J. Sa, G. Smolentsev, M. Szlachetko, J. A. van Bokhoven, J.-C. Dousse, J. Hoszowska, Y. Kayser, P. Jagodzinski, A. Bergamaschi, B. Schmitt, C. David, A. Lücke, *Rev. Sci. Instrum.* **2012**, *83*, 103105.

[23] Z. Németh, J. Szlachetko, É. G. Bajnóczi, G. Vankó, *Rev. Sci. Instrum.* **2016**, *87*, 103105.

[24] P. Glatzel, M. Sikora, G. Smolentsev, M. Ferna, *Catal. Today* **2008**, *145*, 294.

[25] I. Llorens, E. Lahara, W. Delnet, O. Proux, A. Braillard, J. L. Hazemann, A. Prat, D. Testemale, Q. Dermigny, F. Gelebart, M. Morand, A. Shukla, N. Bardou, O. Ulrich, S. Arnaud, J. F. Berar, N. Boudet, B. Cailot, P. Chaurand, J. Rose, E. Doelsch, P. Martin, P. L. Solari, *Rev. Sci. Instrum.* **2012**, *83*, 063104.

[26] D. Sokaras, D. Nordlund, T. C. Weng, R. Alonso Mori, P. Velikov, D. Wenger, A. Garachtchenko, M. George, V.

Borzenets, B. Johnson, Q. Qian, T. Rabedeau, U. Bergmann, *Rev. Sci. Instrum.* **2012**, *83*, 043112.

[27] E. Kleymenov, J. A. van Bokhoven, C. David, P. Glatzel, M. Janousch, R. Alonso-Mori, M. Studer, M. Willimann, A. Bergamaschi, B. Henrich, M. Nachtegaal, *Rev. Sci. Instrum.* **2011**, *82*, 065107.

[28] D. Sokaras, T. C. Weng, D. Nordlund, R. Alonso Mori, P. Velikov, D. Wenger, A. Garachtchenko, M. George, V. Borzenets, B. Johnson, T. Rabedeau, U. Bergmann, *Rev. Sci. Instrum.* **2013**, *84*, 053102.

[29] G. T. Seidler, D. R. Mortensen, A. J. Remesnik, J. I. Pacold, N. A. Ball, N. Barry, M. Styczinski, O. R. Hoidn, *Rev. Sci. Instrum.* **2014**, *85*, 113906.

[30] M. Kavčič, M. Budnar, A. Mühleisen, F. Gasser, M. Žitnik, K. Bučar, R. Bohinc, *Rev. Sci. Instrum.* **2012**, *83*, 033113.

[31] M. R. Alföldi, *Ancient Gold Coins From the Deutsche Bundesbank Collection*, Deutsche Bundesbank, Frankfurt a. M, Giesecke & Devrient, Munich **1983**.

[32] S. Danakas, D. F. Anagnostopoulos. "X-ray tracing for Von-Hamos spectrometers", Poster presentation at the European Conference of X-ray Spectrometry. **2022**.

[33] A. Zymakova´, K. K. Prasad, A. Picchiotti, W. Błachucki, J. Szlachetko, M. Rebarz, J. Uhligc, J. Andreassona, *J. Synchrotron Radiat.* **2020**, *27*, 1730.